PAPER • OPEN ACCESS

Aspects of rf-heating and gas-phase doping of large scale silicon crystals grown by the Float Zone technique

To cite this article: F Zobel *et al* 2018 *IOP Conf. Ser.: Mater. Sci. Eng.* **355** 012006

View the article online for updates and enhancements.

Aspects of rf-heating and gas-phase doping of large scale silicon crystals grown by the Float Zone technique

F Zobel[1], F Mosel[2], J Sørensen[2], P Dold[1]

[1]Fraunhofer CSP, Otto-Eißfeldt-Str. 12, 06120 Halle, Germany;
[2]PVA Crystal Growing Systems GmbH, Im Westpark 10-12, 35435 Wettenberg,

frank.zobel@csp.fraunhofer.de

Abstract. Float Zone growth of silicon crystals is known as the method for providing excellent material properties. Basic principle of this technique is the radiofrequency induction heating, main aspects of this method will be discussed in this article. In contrast to other methods, one of the advantages of the Float Zone technique is the possibility for in-situ doping via gas phase. Experimental results on this topic will be shown and discussed.

1. Introduction

For silicon mono-crystals, the Float Zone (FZ) technique provides material of maximum quality [1–3]. Compared to the Czochralski (Cz) method, the only alternative for large diameter (<4 inch) silicon single crystal growth, the Float Zone material is 2 to 3 orders of magnitude lower in oxygen [4] and shows lower levels of metallic impurities since it is a truly crucible-free technique. The silicon is molten by a radio-frequency inductor placed near the feed rod [5, 6]. FZ silicon is the material of choice for power electronics like thyristors, insulated-gate bipolar transistors (IGBT) or any application where oxygen would lower the performance. Today, the standard diameter is 4" to 6", but 2" or 3" are available as well on the market. Due to physical limitations the maximum diameter is of about 8". Only a few companies world-wide are able to process near this limit.

In the following, important aspects on the basic principles of the FZ technique, i.e. the radiofrequency induction heating, will be discussed. Using the FZ method offers the possibility for in-situ doping via gas-phase. In contrast to other growth methods, uniform axial doping profiles can be produced, by in-situ doping via gas phase during crystallizations. Experimental results together with theoretical considerations will be shown.

2. Experimental setup

The experimental arrangement is shown in Fig.1. The setup is rather simple but the requirements for the mechanical stiffness, the quality and stability of the rf-generator for inductive heating and the accuracy and smoothness of the pulling spindles are very high since the process is very sensitive to vibrations or any sudden impacts. In addition, the specification for the feed rod material is significantly more vigorous than for any other growth techniques [4].

For the experiments, two different Float Zone machines have been used; a smaller one (FZ-14, PVA TePla) for ingots up to 4" and a large one (FZ-35, PVA TePla) for ingots up to 6". For diameters larger than 4" the argon inert gas pressure must be increased, our machine can handle an overpressure of 5 bar. According to the Paschen law, the overpressure reduces the risk of argon ionization caused by the high frequency voltage. Argon ionization is a serious problem and is one of the limitations for larger diameters.
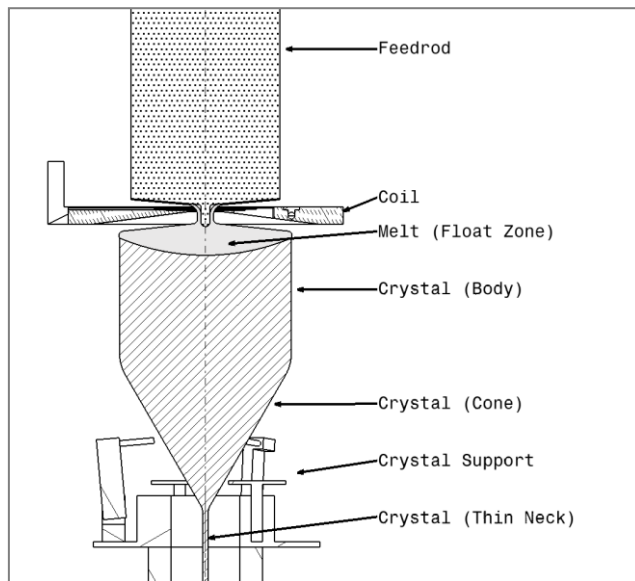
Figure 1. Cross sectional view of the Float-Zone Process. The mono crystal and the feed rod are rotating in opposite directions. The silicon melt flows as a thin film along the bottom side of the feed rod and forms a liquid bridge with the melt lake on top of the growing ingot.

2.1. Radiofrequency Induction Heating

The inductive heating of the silicon feedrod is done with a flat ("pancake") coil with one convolution. It is also referred as "needle eye" inductor, since the inner hole diameter is much smaller than the source rod and the crystal. The radiofrequency current flows with a frequency of 2,5 to 3 MHz and heats the surface of the silicon. Heating at lower frequencies (< 2 MHz) had been analysed, but shows several problems at melting the source rods, mostly the formation of solid silicon spikes [5].

Due to the skin-effect only a small layer of $270 - 290$ μm on the top of the molten silicon is receiving the impact of the dynamic magnetic field [6]. Eddy currents are generated in this layer. The high thermal conductivity of silicon ($\lambda = 148 \frac{W}{m\,K}$) allows the local heat to spread very fast into the bulk material. The skin depth δ_{Sk} can be calculated by

$$\delta_{sk} = \sqrt{\frac{\rho}{\pi * \nu * \mu_0 * \mu_{rel}}} \tag{1}$$

Whereas ρ is the specific resistivity, ν the frequency, μ_{rel} the relative permittivity (for silicon melt ≈ 1,2) and μ_0 the absolute permittivity. Since the conductivity of silicon depends on the amount of base doping and temperature, a detailed look at different cases is necessary.

At 20 °C, undoped solar grade silicon shows a specific resistivity of ≥ 100 Ωcm, electronic grade silicon which comes at even higher purity can reach up to 30 kΩcm of specific resistivity. Heating the silicon leads to a rise in conductivity which also has a strong impact on the penetration of the electrical field. As shown in Fig. 2 the temperature has to rise over a certain level, for the intrinsic carrier mobility to be high enough to enable the required conductivity for inductive heating. The critical temperature is in the range of 400 to 500 °C depending on base doping and size of the specimen [7].
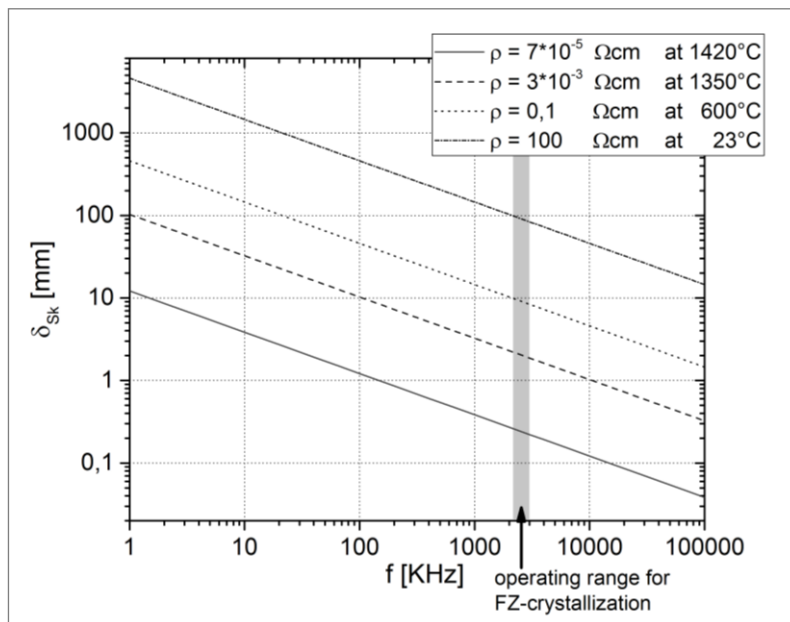
Figure 2. Skin depth depending on used frequency for rf-heating of undoped solar silicon with (R = 100 Ωcm at room temperature). The Resistivity of silicon drops with raising temperature. Resistivity calculated after [7].

To reach this temperature a graphite ring is used to preheat the silicon above this threshold value. Once molten, the conductivity of silicon remains mainly constant, a small change of about 1% can occur [8] but is negligible for further examinations. The efficiency of heating is influenced by the electromagnetic coupling; this can be improved by the shape of the induction coil that follows the melting front as close as possible.

2.2. Doping via gas phase

To influence the resistivity during crystallization an addition of doping gas is required. Phosphine for n-type and diborane for p-type are the common doping gases. For efficient incorporation the doping gas molecules must be in contact with the melt so they are blown directly on the liquid silicon surface. To ensure enrichment in the melt, the doping gas flow must overcome the natural convection in the process chamber as it is shown in Fig. 3. Due to the hot surface of crystal, source rod and the floating zone the surrounding argon gas is heated up as well and streams upwards with maximum velocities of more than 1 m/sec in the inner hole of the inductor where the gas flow is of a turbulent nature. A more laminar and steady upwards flow can be expected on the outer side of the cylindrical crystal and source rod. Streaming velocity is lower in this area. Below the surface of the outer part of the coil, the gas flow is directed radially outwards. Since the optimum contact distance and time of doping gas with the melt surface should be as long as possible, the inlet of doping gas must be pointed crosswise against the natural direction of the stream, so it can reach the free melt surface and stream along it to the inner side of the coil and then along the melting interface over the coil.

To maintain this goal, a certain pressure is required. It translates to a high inlet stream velocity. Therefore the doping gas gets diluted with argon and is blown with an overpressure of ≥ 0,5 bar into the chamber. The flow rate is 200 to 300 ml/min of a mixture consisting of 2 l/min argon gas and 10 to 50 ml/min of diluted doping gas. Since the doping gas is diluted in argon at 100 ppm the finally used gas concentration is ≈ 2,5 ppm. All flow rates are given in norm (milli)litres per minute.

The setup used at the Fraunhofer CSP consists of a small tube with 3 mm inner diameter. The distance between outlet and crystal is about 30 mm. The gas outlet is located at the level of the crystallization interface and points slightly upwards (Fig. 3).

Doping efficiency η_D can be calculated after:

$$\eta_D = \frac{a\dot{t}_C}{n*a\dot{t}_G} = \frac{\dot{V}_C*C_C}{\dot{V}_G*C_G*\frac{1}{V_m}*N_A} = \frac{\emptyset_C^2*\frac{\Pi}{4}*v_c*C_C}{\dot{V}_G*C_G*\frac{1}{V_m}*N_A} \tag{2}$$

Where the ratio $\frac{a\dot{t}_C}{n*a\dot{t}_G}$ stands for the flow of atoms that are incorporated into the crystal divided by the flow of dopant atoms going into the chamber. The factor $n = 2$ for diborane (B_2H_6) and $n=1$ for phosphine (PH_3), since diborane consists of two boron atoms per molecule. $\dot{V}_C$ is the volume flow of crystalline silicon that is calculated based on the diameter of the crystal $\emptyset_C$ and the crystallization rate v_c. It is multiplied with the concentration of dopant atoms in the crystal C_C, that can be calculated from the crystal resistivity [9]. $\dot{V}_G$ stands for the gas volume flow of the doping gas, C_G for the concentration of pure doping gas in the mixture (in this case ≈100 ppm), V_m is the molecular volume and N_A the Avogadro constant.
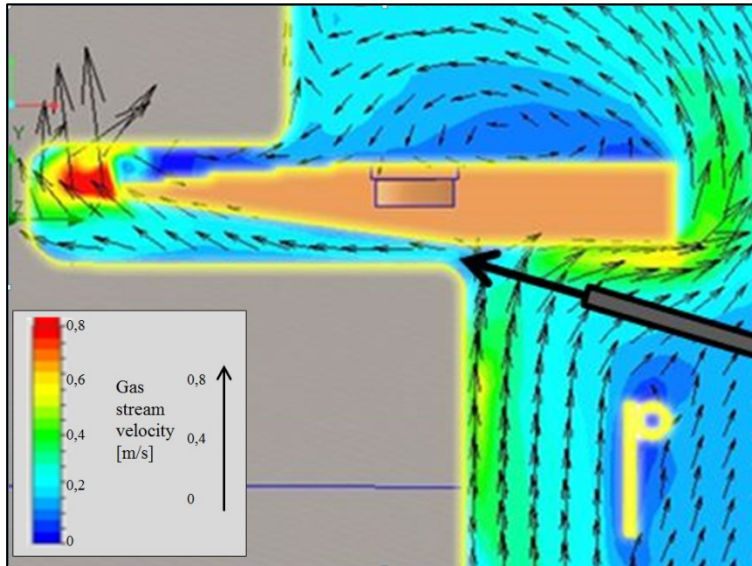

Figure 3. Positioning of doping gas inlet; at a high flow velocity the doping gas stream perpendicular to the natural convection to the free melt surface then it is taken along with the gas flow along the silicon surface through the coil hole in an inwards direction, and then outwards along the melting front for efficient incorporation. (CFD simulation carried out with FlowEFD by PVA Tepla).

3. Results

3.1. P-type doping with diborane (B_2H_6)
Investigations of doping of a 5 inch crystal via gas phase and diborane were conducted. The diborane gas flow was enabled after the starting cone of the crystal and set to a value of 50 ml/l, with an argon flow rate of 2 l/min and an overpressure of 0,5 bar (Fig.4). The specific resistivity of the grown crystal was measured with an eddy current sensor and cross checked via four point probe measuring. The crystal position could be determined by assigning it to the lower spindle position that is logged during the growth process.

The specific resistivity at the beginning of the crystal (up to 300 mm length, see Fig. 4) was about 600 Ωcm, an undoped source rod was used for crystallization. Immediately after enabling the gas flow a drop in resistivity of the crystal to 50 Ωcm is observed. That equals a rise in boron concentration of the crystal form $2,2 * 10^{13}$ at/cm³ to $2,6 * 10^{14}$ at/cm³. As can be seen in Fig. 4 an asymptotic drop to 7 Ωcm (equals $1,9 * 10^{15}$ at/cm³) follows. It takes 100 mm of grown crystal length to reach this equilibrium state.
The ratio of boron atoms blown into the chamber and resulting boron atom concentration in the crystal equals to 24,5 %, considering the crystallization velocity of 3 mm/ min. Nearly every 4th atom of boron that is blown into the chamber is incorporated into the melt. The rather low value is not

surprising, since diborane is thermal unstable an starts decomposing already at 100 °C in hydrogen and other borane complexes like B_4H_{10}, B_5H_9, B_5H_{11}, $B_{10}H_{14}$ or higher molecular solid yellow boron $(BH_{\approx 1})_x$ [10]. After a longer process time elementary boron can be seen as dark brown film covering the gas nozzle.

3.2. N-type doping with phosphine (PH3)

Just as the p-type doping, the n-type variation was analyzed at a 5 inch crystal which was grown with a speed of 3 mm/min. The starting cone was grown without doping to have a reference value of specific resistivity. The source rod was different to the first one but undoped as well. It resulted in a specific crystal resistivity of 120 Ωcm ($3,6 * 10^{13}$ at/cm³). In this experiment the amount of phosphine gas flow rate was ramped up in three steps, from 0 to 30, 40 and finally 50 ml/min. This can be seen in Fig 5. The corresponding resistivity measured at 12, 7, and 3 Ωcm ($3,7 * 10^{14}$ at/cm³; $6,4 * 10^{14}$ at/cm³ and $1,5 * 10^{15}$ at/cm³). The absorption rate was determined based on this values is 42,5 %, nearly every second phosphorus atom is incorporated in the crystal. Phosphine is more thermally stable than diborane, its decomposition temperature is about 500 °C [11]. Better doping efficiency was expected and could be proven. Since the necessary amount of dopant atoms in silicon is lower in n-type due to the higher mobility of the free electrons in the crystal lattice, a lower amount of phosphorus is required for the same resistivity compared to p-type.

Still, the amount of incorporated atoms is low, compared to values from modelling of a 4 inch process that predict a dopant efficiency of up to 95 % [12]. Reasons for these differences might be the evaporation of phosphorus due to the high partial pressure, but this is supposed to be rather low due to the high chemical affinity of phosphorus and silicon. Another difference that might explain the deviations is the coil designs. A relatively small inductor hole compared to the simulated process in [12] might supress the gas flow next to the floating zone. The dopant concentration in the gas flowing along the melting surface in the area above the coil might be lowered, due to this reason.

For both, p- and n-type doping the incorporation ration of dopants might be increased with a higher outlet velocity and less distance. The inlet flow rate can be increased by using a higher doping gas pressure. A smaller diameter of the gas inlet or a nozzle with reduced exhaust area even increases the doping gas inlet velocity and can improve the amount of doping gas molecules reaching the melt surface. The distance can be reduced as well, but to prevent arcing, the tube or nozzle should be of an insulating material, e.g. quartz, that is also resistant to the occurring high temperatures from the radiating silicon melt and crystal.
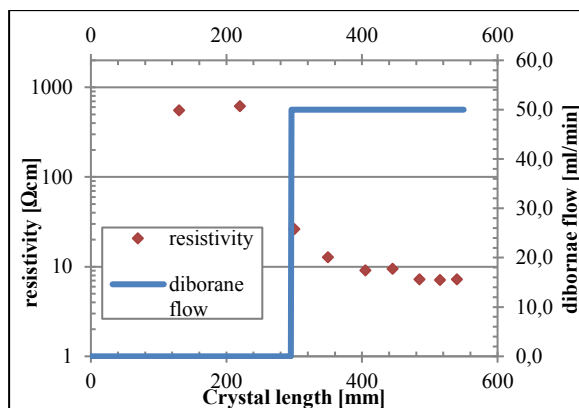

Figure 4. P-type doping via gas phase with diborane resistivity of a 5 inch FZ-crystal (grown with 3,0 mm/min) in axial direction.
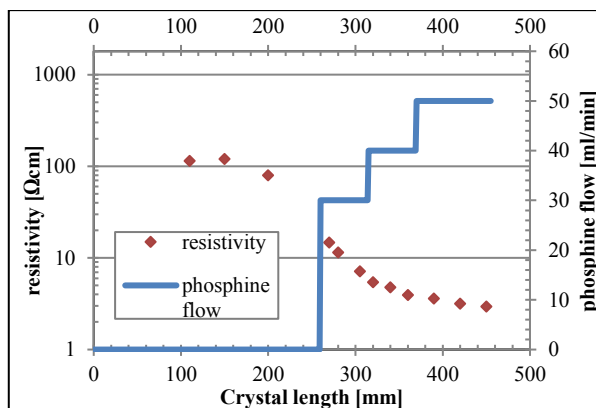

Figure 5. N-Type doping via gas phase with phosphine resistivity of a 5 inch FZ-Crystal (grown with 3,0 mm/min) in axial direction.

4. Conclusions

In the article we have shown important aspects and considerations on radiofrequency induction heating. The temperature dependence of the conductivity of silicon, and its impact on the skin depth was discussed. This leads to the requirement of high working frequencies.

Experiments on gas-phase doping have been carried out, showing a doping efficiency of 25 % (43 %) for diborane (phosphine) in the current experimental setup. The influence of the gas-flow on the resistivity has been shown. The reached efficiency shows a much smaller value than simulations suggest, deviations are discussed. A smaller tube or a nozzle in closer proximity to the melt with higher doping gas pressure might increase the ration of doping atoms blown in the chamber to doping atoms incorporated in the crystal. Further investigations will provide additional data to confirm these assumptions.

Acknowledgement

References

[1]   Rost H J, Luedge A, Riemann H, Kirscht F and Schulze F W 2012 *Crystal Research and Technology* **47** 273–8

[2]   Ciszek T F and Wang T H 2000 *Proceedings of SPIE - The International Society for Optical Engineering* **4218** 105–17

[3]   Dold P 2015 *Semiconductors and Semimetals* **92** 1–61

[4]   Zobel F, Dold P, Kunert R, Lauer K and Michl B 2014 *Float Zone Kristallzüchtung für Solare Anwendungen (Deutsche Kristallzuechtungstagung)* (Halle (Saale))

[5]   Rost H J, Menzel R, Luedge A and Riemann H 2012 *Journal of Crystal Growth* **360** 43–6

[6]   Hurle D T J (ed) 2016 *Bulk Crystal Growth: A. Basic Techniques (Handbook of Crystal Growth)* (Saint Louis: Elsevier Science)

[7]   Li S S 1977 *The dopant density and temperature dependence of electron mobility and resistivity in n-type silicon (Semiconductor Measurement Technology* 400-33*)* (Washington, D.C.: National Bureau of Standards)

[8]   Sasaki H, Ikari A, Terashima K and Kimura S 1995 *Japanese Journal of Applied Physics, Part 1: Regular Papers and Short Notes and Review Papers* **34** 3426–31

[9]   National Bureau of Standards 1981 The relationship between resistivity and dopant density for phosphorus-and boron-doped silicon *(*400-64*)* (Washington, D.C.: U.S. Department of Commerce) (accessed 13 Jan 2017)

[10]   Holleman A F, Wiberg E and Wiberg N 2007 *Lehrbuch der anorganischen Chemie* 102nd edn (Berlin: De Gruyter)

[11]   Baillargeon J N, Cheng K Y, Jackson S L and Stillman G E 1991 *Journal of Applied Physics* **69** 8025–30

[12]   Sabanskis A, Surovovs K and Virbulis J 2017 *Journal of Crystal Growth* **457** 65–71